

Anti-diffracting beams through the diffusive optical nonlinearity

F. Di Mei,^{1,2} J. Parravicini,^{1,3} D. Pierangeli,¹ C. Conti,⁴ A. J. Agranat,⁵
and E. DelRe^{1,3,*}

¹ Department of Physics, University of Rome "La Sapienza", 00185 Rome, Italy

² Center for Life Nano Science@Sapienza, Istituto Italiano di Tecnologia, 00161 Rome, Italy

³ IPCF-CNR, University of Rome "La Sapienza", 00185 Rome, Italy

⁴ Institute for Complex Systems, National Research Council (ISC-CNR), Via dei Taurini 19,
00185 Rome, Italy

⁵ Applied Physics Department, Hebrew University of Jerusalem, 91904 Israel

*eugenio.delre@uniroma1.it

Abstract: Anti-diffraction is a theoretically predicted nonlinear optical phenomenon that occurs when a light beam spontaneously focalizes independently of its intensity. We observe anti-diffracting beams supported by the peak-intensity-independent diffusive nonlinearity that are able to shrink below their diffraction-limited size in photorefractive lithium-enriched potassium-tantalate-niobate (KTN:Li).

© 2014 Optical Society of America

OCIS codes: (190.4400) Nonlinear optics, materials; (190.5330) Photorefractive optics; (260.5950) Self-focusing.

References and links

1. M. Born and E. Wolf, *Principles of Optics*, 6th ed. (Pergamon, 1980).
2. J. M. Cowley, *Diffraction Physics*, 3rd ed. (Elsevier Science B.V., Amsterdam, 1995).
3. R. W. Boyd, S. G. Lukishova, and Y. R. Shen (Eds.), *Self-Focusing: Past and Present*, (Springer, New York 2009).
4. S. Trillo and W. Torruellas (Eds.), *Spatial Solitons* (Springer, Berlin, 2001).
5. Z. G. Chen, M. Segev, and D. N. Christodoulides, "Optical spatial solitons: historical overview and recent advances," *Rep. Prog. Phys.* **75**, 086401 (2012).
6. H. Kosaka, T. Kawashima, A. Tomita, M. Notomi, T. Tamamura, T. Sato, and S. Kawakami, "Self-collimating phenomena in photonic crystals," *Appl. Phys. Lett.* **74**, 1212–1214 (1999).
7. H. S. Eisenberg, Y. Silberberg, R. Morandotti, and J. A. Aitchison, "Diffraction management," *Phys. Rev. Lett.* **85**, 1863–1866 (2000).
8. K. Staliunas and R. Herrero, "Nondiffractive propagation of light in photonic crystals," *Phys. Rev. E* **73**, 016601 (2006).
9. O. Firstenberg, P. London, M. Shuker, A. Ron, and N. Davidson, "Elimination, reversal and directional bias of optical diffraction," *Nat. Phys.* **5**, 665–668 (2009).
10. D. N. Christodoulides and T. H. Coskun, "Diffraction-free planar beams in unbiased photorefractive media," *Opt. Lett.* **21**, 1460–1462 (1996).
11. B. Crosignani, E. DelRe, P. Di Porto, and A. Degasperis, "Self-focusing and self-trapping in unbiased centrosymmetric photorefractive media," *Opt. Lett.* **23**, 912–914 (1998).
12. B. Crosignani, A. Degasperis, E. DelRe, P. DiPorto, and A. J. Agranat, "Nonlinear optical diffraction effects and solitons due to anisotropic charge-diffusion based self-interaction," *Phys. Rev. Lett.* **82**, 1664–1667 (1999).
13. E. DelRe, M. Tamburrini, M. Segev, R. Della Pergola, and A. J. Agranat, "Spontaneous self-trapping of optical beams in metastable paraelectric crystals," *Phys. Rev. Lett.* **83**, 1954–1957 (1999).
14. E. DelRe, E. Spinozzi, A. J. Agranat, and C. Conti, "Scale-free optics and diffractionless waves in nanodisordered ferroelectrics," *Nat. Photonics* **5**, 39–42 (2011).
15. C. Conti, A. J. Agranat, and E. DelRe, "Subwavelength optical spatial solitons and three-dimensional localization in disordered ferroelectrics: Toward metamaterials of nonlinear origin," *Phys. Rev. A* **84**, 043809 (2011).
16. J. Parravicini, F. Di Mei, C. Conti, A.J. Agranat, and E. DelRe "Diffraction cancellation over multiple wavelengths in photorefractive dipolar glasses," *Opt. Express* **19**, 24109–24114 (2011).

17. V. Folli, E. DelRe, and C. Conti “Beam Instabilities in the Scale-Free Regime,” *Phys. Rev. Lett.* **108**, 033901 (2012).
18. A. A. Bokov and Z. -G. Ye, “Recent progress in relaxor ferroelectrics with perovskite structure,” *J. Mater. Sci* **41**, 31–52 (2006).
19. A. Gumennik, Y. Kurzweil-Segev, and A. J. Agranat, “Electrooptical effects in glass forming liquids of dipolar nano-clusters embedded in a paraelectric environment,” *Opt. Mat. Express* **1**, 332–343 (2011).
20. E. DelRe and C. Conti, “Scale-Free Optics,” *Nonlinear Photonics and Novel Optical Phenomena*, Z. Chen and R. Morandotti (Eds.) (Springer, New York, 2012).
21. A. Agranat, R. Hofmeister, and A. Yariv, “Characterization of a new photorefractive material $K_{1-y}LyT_{1-x}Nx$,” *Opt. Lett.* **17**, 713–715 (1992).
22. Y-C.Chang, C. Wang, S. Yin, R. C. Hoffman, and A. G. Mott, “Giant electro-optic effect in nanodisordered KTN crystals,” *Opt. Lett.* **38**, 4574–4577 (2013).
23. J. Parravicini, C. Conti, A. J. Agranat, and E. DelRe, “Programming scale-free optics in disordered ferroelectrics,” *Opt. Lett.* **37**, 2355–2357 (2012).
24. J. Parravicini, A. J. Agranat, C. Conti, and E. DelRe, “Equalizing disordered ferroelectrics for diffraction cancellation,” *Appl. Phys. Lett.* **101**, 111104 (2012).
25. Y-C. Chang, C. Wang, S. Yin, R. C. Hoffman, and A. G. Mott, “Kovacs effect enhanced broadband large field of view electro-optic modulators in nanodisordered KTN crystals,” *Opt. Express* **21**, 17760–17768 (2013).
26. J. Parravicini, D. Pierangeli, F. DiMei, A. J. Agranat, C. Conti, and E. DelRe, “Aging solitons in photorefractive dipolar glasses,” *Opt. Express* **21**, 30573–30579 (2013).
27. D. Pierangeli, J. Parravicini, F. DiMei, GB. Parravicini, A. J. Agranat, and E. DelRe, “Photorefractive light needles in glassy nanodisordered KNTN,” *Opt. Lett.* **39** 1657–1660 (2014).
28. A. Yariv and P. Yeh, *Optical Waves in Crystals* (Wiley, New York 1984).
29. F. Jona and G. Shirane, *Ferroelectric Crystals* (Dover, New York 1993).

1. Introduction and motivation

Diffraction causes light beams to spread out, losing spatial definition and intensity [1, 2]. This forms a limit to the spatial resolution of optical imaging systems based on far-field optics, such as a standard wide-area microscope. In nonlinear materials, self-focusing can change this spreading, but the effect is intrinsically peak-intensity dependent [3]. When self-focusing exactly balances beam spreading caused by diffraction, something that imposes a precise peak-intensity beam-width relationship, stable non-spreading beams in the form of spatial solitons appear [4, 5].

Experiments in waveguide arrays and photonic crystals have shown that interference can cause beams in specific directions to suffer a cancelled diffraction [6–8]. In electro-magnetic-induced transparency experiments, interference can even lead to inverted (or negative) diffraction [9]. Based on interference, this modified diffraction occurs along specific directions and for beams with a small angular spectrum. A more general effect would be the observation of beams that literally “anti-diffract” as they propagate in a substance. In such a system, beams will naturally converge instead of spreading, irrespective of direction of propagation and for a wide range of beam sizes, even with a considerable angular spectrum. In distinction to self-focusing, that depends on intensity and generally becomes stronger as beams shrink, anti-diffraction should be intensity-independent.

Studies in nanodisordered photorefractive crystals have shown that the diffusive nonlinearity in paraelectric samples [10–13] can strongly reduce natural diffraction, ultimately cancelling it, a phenomenon known as scale-free optics [14–17].

In this paper we theoretically predict anti-diffraction supported by the diffusive nonlinearity and report its first observation in lithium-enriched potassium-tantalate-niobate (KTN:Li).

2. Theoretical

In a photorefractive crystal, light absorbed by deep in-band impurities diffuses and gives rise to a static electric field $E_{dc} = -(k_B T/q)\nabla I/I$, where k_B is the Boltzmann constant, T the crystal temperature, q the elementary charge, $I = |A|^2$ the optical intensity, and A the optical field

amplitude [10–13]. When the crystal is a disordered ferroelectric above its peak temperature T_m [18], the electro-optic response of the mesoscopic dipoles (polar-nanoregions - PNRs) [19] gives rise to a scalar change $\Delta n = -(n_0^3/2)g\varepsilon_0^2\chi_{PNR}^2|\mathbf{E}_{dc}|^2$ in the background index of refraction n_0 [20], where χ_{PNR} is the PNR low-frequency susceptibility, g is the electro-optic coefficient, and $L = 4\pi n_0^2\varepsilon_0\sqrt{g}\chi_{PNR}(k_B T/q)$ [14, 15]. In the paraxial approximation, the slowly varying optical amplitude A obeys the equation

$$2ik\frac{\partial A}{\partial z} + \nabla_{\perp}^2 A - \frac{L^2}{\lambda^2} \left(\frac{\nabla_{\perp}|A|^2}{2|A|^2} \right)^2 A = 0, \quad (1)$$

where $k = k_0 n_0$, $k_0 = 2\pi/\lambda$, z is the propagation axis, $\nabla_{\perp} \equiv (\partial_x, \partial_y)$, and λ is the optical wavelength. Separating the variables, $A(x, y, z) = \alpha(x, z)\beta(y, z)$, α must obey

$$2ik\frac{\partial \alpha}{\partial z} + \frac{\partial^2 \alpha}{\partial x^2} - \frac{L^2}{\lambda^2} \frac{(\partial_x |\alpha|^2)^2}{4|\alpha|^4} \alpha = 0. \quad (2)$$

The same equation holds for β replacing x with y . Eq. (2) is satisfied by the solution

$$\alpha(x, z) = \frac{\alpha_0}{\sqrt{w_x(z)}} e^{-\frac{x^2}{w_x(z)} + i[\phi_0(z) + \frac{1}{2}\phi_2(z)x^2]} \quad (3)$$

with

$$\phi_0(z) = -\frac{1}{kw_{0x}^2} \frac{\tan^{-1}(\sqrt{az})}{\sqrt{a}} \quad (4)$$

and

$$\phi_2(z) = \frac{az}{1+az^2}. \quad (5)$$

Here $a \equiv (1 - L^2/\lambda^2)/k^2 w_{0x}^4$, w_{0x} is the initial beam in the x -direction, and α_0 is a constant. For a round launch beam with $w_{0x} = w_{0y} = w_0$, the waist in two transverse dimensions along the propagation direction z is given by

$$w(z) = w_0 \sqrt{1 + \frac{4}{k^2 w_0^4} \left[1 - \left(\frac{L^2}{\lambda^2} \right) \right] z^2}. \quad (6)$$

For $L > \lambda$, Eq.(6) foresees beams that shrink into a point-like focus at a characteristic "collapse length"

$$z_c = \frac{n\pi w_0^2}{\lambda} \frac{1}{\sqrt{(L/\lambda)^2 - 1}}, \quad (7)$$

independently of intensity.

3. Experimental

To experimentally demonstrate diffusive anti-diffraction described by Eq.(6) we use the setup illustrated in Fig. 1. A 0.8 mW (before L3) He-Ne laser operating at $\lambda = 632.8\text{nm}$ is expanded and subsequently focused down to a spot with an $w_0 = 7.8\mu\text{m}$ (intensity full-width-at-half-maximum of $\Delta x = \Delta y \simeq 9.4\mu\text{m}$) at the input face of a sample of lithium-enriched potassium-tantalate-niobate (KTN:Li). The composite ferroelectric is grown through the top-seeded solution method so as to have a peak dielectric maximum T_m at room temperature and high optical quality [21]. Our specific crystal is a zero-cut $2.6 \times 3.0 \times 6.0$ mm sample with a composition of

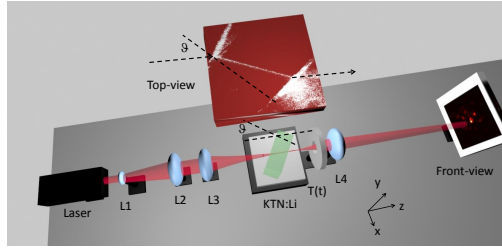


Fig. 1. Anti-diffraction setup. A He-Ne laser operating at 633 nm is enlarged through lenses L1 and L2 and focused down to an $8 \mu\text{m}$ spot at the input facet of the KTN:Li sample, rotated with the respect to the propagation axis z by a variable angle θ and brought through a temperature cycle $T(t)$. (Front-view) The input and output facets are imaged through lens L4 onto a CCD camera. (Top-view) Scattered light is captured above the sample and imaged, through a microscope, onto a second CCD camera.

$\text{K}_{1-x}\text{Ta}_{1-y}\text{Nb}_y\text{O}_3:\text{Li}_x$ with $x = 0.003$, $y = 0.36$. Cu impurities (approximately 0.001 atoms per mole) support photorefraction in the visible, whereas focusing and cross-polarizer experiments give $n_0 = 2.2$ and $g = 0.14\text{m}^4\text{C}^{-2}$. The beam is polarized in the x direction and propagates inside the crystal for a distance of $L_z \simeq 3.0\text{mm}$. The crystal is rotated to a desired angle θ in the x, z plane. The output intensity distribution of the beam is imaged by a CCD camera through an imaging lens ($\text{NA} \simeq 0.35$). Light scattered in the vertical y direction is captured by a second CCD camera placed above the sample in the y direction through a high aperture microscope ($\text{NA} \simeq 0.8$) positioned so as to image the plane of propagation.

We are able to achieve $L > \lambda$ during a transient by operating near $T_m = 287.5\text{K}$, identified through dielectric constant measurements, and enacting a non-monotonic temperature trajectory $T(t)$ [22–27]. In fact, considering the values of n_0 , g , and $k_B T/q \simeq 25 \text{ mV}$, $L \sim \lambda$ for $\chi_{PNR} \sim \lambda / (4\pi n_0^2 \epsilon_0 \sqrt{g} (k_B T/q)) \simeq 10^5$, i.e., an anomalously large value of susceptibility only observable in proximity of the dielectric peak. In each anti-diffraction experiment we enacted the following procedure: the crystal was first cleaned of photorefractive space-charge by illuminating it with a fully powered microscope illuminator placed at approximately 0.1 m above the crystal for over 10 minutes. Using a temperature controller that drives the current of a Peltier junction placed directly below the crystal in the y direction, we brought the sample to thermalize at $T_A = 303\text{K}$. The sample is then cooled from $T_A = 303\text{K}$ at the rate of 0.07 K/s to a temperature T_D (that is fixed to different values in experiments, see below), where it is kept for 60 s. Then the sample is heated once again at a rate of 0.2 K/s to the operating temperature ($> T_D$) $T_B = 290\text{K}$. The strong transient response is observed to have a characteristic response time of 10–30 s, with measured values of collapse length $z_c = 3.9 - 6.8\text{mm}$ that depend on the actual value of T_D used. This regime is not otherwise accessible with our apparatus by a standard rapid cooling (i.e., from T_A directly to T_B). Once T_B is reached, the temperature cycle $T(t)$ is complete and we switched on the laser beam, recording top-view and front view images of the captured intensity distribution. All intervals of time t are indicated such that the laser is turned on at $t = 0$.

4. Results

In Fig. 2 we show a condition of strong anti-diffraction observed when $T_D = 283\text{K}$. As shown in Fig. 2(a-c), the $w_0 = 7.8\mu\text{m}$ input beam diffracts to $38 \mu\text{m}$ as it propagates to the output facet at the initial $T_A = 303\text{K}$. After the cooling/heating cycle, the output beam shrinks to $5 \mu\text{m}$ ($L \simeq 0.643\mu\text{m}$). Snapshots of the top-view scattered light illustrate the transition from the

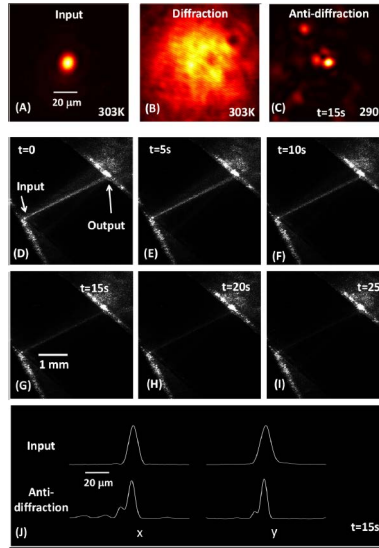


Fig. 2. Strong anti-diffraction for $T_D = 283\text{K}$. The input $800\ \mu\text{W}$ $8\ \mu\text{m}$ Gaussian beam (a) diffracts to $38\ \mu\text{m}$ at $T_A = 303\text{K}$ (b). It then shrinks after 15 s to a waist of $5\ \mu\text{m}$ (c), before relaxing once again into a strongly spreading beam. (d)-(i) Top-view images captured through a high-aperture microscope of the stray light emitted by the beam showing the transition, in time, from a diffracting (d) to an anti-diffracting beam (g), and once again to a diffracting one (i). (j) Intensity profiles of the input beam compared to the anti-diffracting beam at $t = 15\text{s}$.

diffracting Fig. 2(d-f) to the shrinking beam condition Fig. 2(g), and ultimately to the once again spreading phase Fig. 2(h-i) with strongly reduced scattering. In this case, the crystal is rotated by $\theta = 11^\circ$. The beam profiles of the input and output distributions (at $t = 15\text{s}$) are compared in Fig. 2(j). From Eqs.(6-7) we deduce a value of $z_c = 3.9\text{mm}$. To confirm the approximate intensity-independent and angle-independent nature of the effect, we repeated the experiment with different levels of beam power and propagation angles. We found same levels of anti-diffraction repeating experiments with 8, 30, 240, $800\ \mu\text{W}$ beams and for launch angles $\theta = 5^\circ - 11^\circ$. For example, at a fixed angle $\theta = 11^\circ$, increasing the beam power from $30\ \mu\text{W}$ and $240\ \mu\text{W}$, alters the minimum waist by less than 12%. In turn, at $\theta = 5^\circ$, for beam powers from $30\ \mu\text{W}$ and $240\ \mu\text{W}$, the minimum waist of the antidiffracting beams varies by less than 14%. The only relevant systematic effect associated with different beam powers was a lengthening of the anti-diffraction response time, as expected for the cumulative nature of the photorefractive response.

In Fig. 3 we show a condition of weaker anti-diffraction from 7.8 to 7 microns when $T_D = 286\text{K}$, ($L \simeq 0.636\ \mu\text{m}$). Here from Eqs.(6-7) $z_c = 6.8\text{mm}$, and the maximum anti-diffraction occurs after 10 s from the end of the thermal cycle.

In Fig. 4 we show the time sequence for the two reported cases of Fig. 2 and Fig. 3. The transverse intensity distribution is shown for different intervals of time t from the completion of the temperature cycle and the launching of the laser beam, highlighting the transient nature of the anti-diffraction.

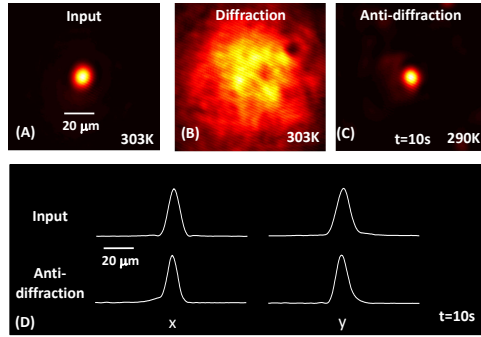


Fig. 3. Weak anti-diffraction for $T_D = 286\text{K}$. The input $7.8\ \mu\text{m}$ beam (a) diffracts as in the previous case (b) and shrinks to $7\ \mu\text{m}$ after 10 s (c). (d) Profiles of input and anti-diffraction beams (at $t = 10\text{s}$).

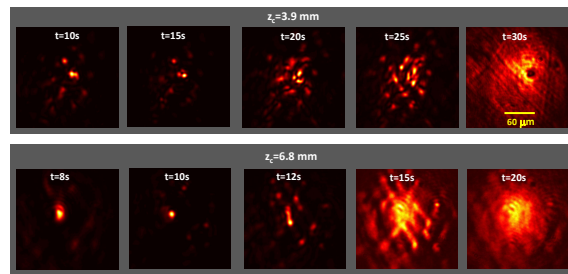


Fig. 4. Time sequence of the anti-diffraction. Output intensity distributions at different instants of time showing the decay of the anti-diffraction regime and the formation of transient spatial patterns in the cases of strong (Top) and weak (Bottom) anti-diffraction.

5. Conclusion

Anti-diffraction is a new nonlinear intensity-independent wave phenomenon that can possibly lead to new ideas in imaging techniques. From a purely fundamental perspective, we note that our paraxial theory will break down if $L_z \simeq z_c$, where the strong-focusing requires a fully non-paraxial treatment, so that future experiments with shorter z_c or longer L_z may hold further novel effects. Moreover, one phenomenological aspect that already at this stage of anti-diffraction merits discussion is the formation of transient patterns after the strong anti-diffraction stage, as reported in Fig. 4. The patterns are more evident as the value of z_c decreases and are not strongly dependent on θ for the range $\theta = 5 - 22^\circ$ we scanned. Since this excludes the possible influence of ferroelectric domains, which are pinned to the principal axes of the crystal in its nominal paraelectric $m3m$ phase [28, 29], these patterns appear an effect of the nonlinear (but peak-intensity-independent) propagation itself.

Acknowledgments

Funding from grants PRIN 2012BFNWZ2, Sapienza Ricerca 2012 and Award 2013 are acknowledged. A.J.A. acknowledges the support of the Peter Brojde Center for Innovative Engineering.